Supplementary Information

Constructing Oxygen Vacancies in Anatase TiO2: Enhancing Acetylene Semi-Hydrogenation Performance through H_2 Heterolytic Cleavage

Qianjun Zhang,‡[a] Chong Yao,‡[a] Fan Zhang,[a] Yicheng Chen,[a] Zile Li,[a] Yongkang Zhou,[a] Yingxue Qin,[a] Longyu Xu,[a] Feng Feng,[a] Jia Zhao,[a] Chunshan Lu,[a] Qunfeng Zhang,*[a] Qingtao Wang*[a] and Xiaonian Li*[a]

[a] Industrial Catalysis Institute of Zhejiang University of Technology, State Key Laboratory Breeding Base of Green Chemistry-Synthesis Technology, Hangzhou,310014, P. R. China

‡ These authors contributed equally to this work.

*Corresponding author: Prof. Qunfeng Zhang (zhangqf@zjut.edu.cn), Prof. Qingtao Wang (qtwang@zjut.edu.cn), Prof. Xiaonian Li (xnli@zjut.edu.cn).

1. Computer details

All the models for the hydrogenation of acetylene to ethylene are carried out within the framework of the Perdew-Burke-Ernzerhof (PBE) method of generalized gradient approximation (GGA) in the Vienna ab initio simulation program (VASP)[1, 2]. Spin polarization is considered throughout the calculations. A 1 × 1 × 1 Monkhorst-Pack k-point mesh was used.The vacuum layer was set to 15 Å to avoid interactions between neighboring surfaces. Van der Waals force interactions between molecules are considered. Differential charge data are processed using VESTA software[3]

2. Calculation of reaction rate and apparent activation energy

The acetylene reaction rate (r, mol·s^{-1}·g_{cat}^{-1}) was calculated according to the following equations:

$$r = \frac{X \times F}{m}$$

where X = Acetylene conversion, %

F = Acetylene molar flow rate, mol·s^{-1}

m = weight of catalysts, g

The ethylene production rate ($r_{C_2H_4}$, mol·s^{-1}·g_{cat}^{-1}) was calculated according to the following equations:

$$r_{C_2H_4} = r \times S_{C_2H_4}$$

where r = acetylene reaction rate, mol·s^{-1}·g_{cat}^{-1}

$S_{C_2H_4}$ = Selectivity of ethylene, %

Carbon balance calculation：

$$carbon\ blance = \frac{2F_{out,\ C_2H_2} + 2F_{out,\ C_2H_4} + 2F_{out,\ C_2H_6} + 4F_{out,\ C_4}}{2(F_{in,\ C_2H_2} + F_{in,\ C_2H_4})} \times 100\%$$

Where $F_{out,\ C_2H_2}$= The rate of acetylene flow out after the reaction, mol·s^{-1}

$F_{out,\ C_2H_4}$= The rate of ethylene flow out after the reaction, mol·s^{-1}

$F_{in,\ C_2H_4}$= The rate of ethylene flow entering before the reaction, mol·s^{-1}

$F_{out,\ C_2H_6}$= The rate of ethane flow out after the reaction, mol·s^{-1}

$F_{out,\ C_4}$= The rate of C_4 flow out after the reaction, mol·s^{-1}

$F_{in,\ C_2H_2}$= The rate of acetylene flow entering before the reaction, mol·s^{-1}

The apparent activation energy (Ea) was calculated using the Arrhenius formula under toluene conversion below 15%:

$$lnr = -\frac{E_a}{RT} + lnA$$

where R = ideal gas constant, 8.314 J·mol^{-1}·K^{-1}

r = reaction rate of acetylene, mol·s^{-1}·g_{cat}^{-1}

T = reaction temperature, K

ln A = a constant

Finally, Ea was obtained by using the slope of the linear plot of 1000/T versus ln r.

3. Internal and external mass transfer limitations

3.1 Internal Diffusion

To ensure the reaction rates fall within the intrinsic kinetic regime, it is necessary to eliminate the effects of both external and internal diffusion. Given that TiO_2 catalysts treated under different atmospheres exhibit varying specific surface areas (see Table S1), we conducted experiments to eliminate internal and external diffusion for T-600, T-200, T-H200, and T-H600, which have different O_V contents. In a fixed-bed reactor, the elimination of external mass transfer effects is typically achieved by varying the linear flow velocity while maintaining a constant space velocity. Specifically, this involves simultaneously increasing the flow rate and the catalyst mass to test the reaction rate. When the reaction rate remains unchanged despite changes in the flow rate, the influence of external mass transfer can be considered negligible.[4] Therefore, we investigated the influence of external mass transfer on T-H200, T-H600, T-200, and T-600 under the conditions of a space velocity of 54,000 h^{-1}, H_2: C_2H_2 = 10:1, a reaction temperature of 250°C, and a reaction pressure of 101 kPa. After stabilizing the catalysts for 2 hours, kinetic data were collected three times for each flow rate and each catalyst, with the average values reported. The experimental results are shown in **Fig. S1a.**

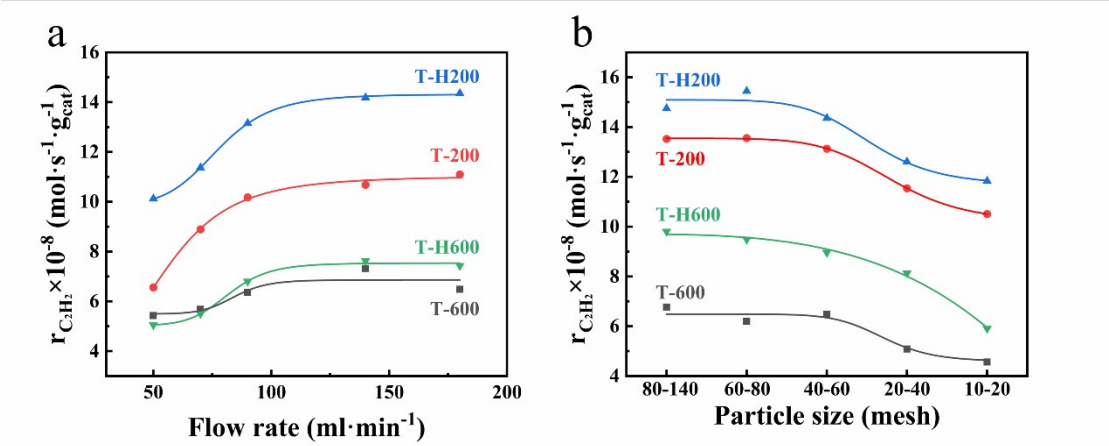

Fig. S1. (a) The effect of different feed flow rates and (b) The effect of different particle sizes on the acetylene reaction rate over TiO_2 catalysts with varying O_V content was investigated under constant space velocity (reaction conditions: T = 250°C, Sv = 54000 h^{-1}, H_2: C_2H_2 = 10:1, P = 101 kPa).

Fig. S1 shows that as the feed flow rate increases from 50 to 90 mL·min^{-1}, the reaction rate for all TiO_2 catalysts with different O_V contents increases significantly, indicating a substantial impact of external diffusion. However, when the flow rate exceeds 90 mL·min^{-1}, the reaction rate increases slowly and stabilizes, demonstrating that external mass transfer limitations can be eliminated at flow rates above 90 mL·min^{-1}. Therefore, to ensure accuracy, a flow rate of 140 mL·min^{-1} was chosen for the subsequent kinetic experiments.

When the diffusion rate of the reactant gases within the catalyst's pore structure is sufficiently slow, internal diffusion becomes the rate-limiting step in the catalytic reaction. In this case, the catalyst's performance does not reflect its intrinsic catalytic

activity. The macroscopic reaction rate inferred from the results is also a composite of the internal diffusion rate and the reaction rate. Therefore, the impact of internal mass transfer on the study of intrinsic catalyst kinetics cannot be overlooked. In heterogeneous catalysis, internal mass transfer effects are typically investigated by varying the catalyst particle size.[4, 5] When the reaction rate shows minimal dependence on particle size, it indicates that internal mass transfer effects can be considered negligible. To eliminate the influence of internal diffusion, we conducted experiments under the following conditions: a feed gas flow rate of 140 mL·min^{-1}, space velocity of 54,000 h^{-1}, H_2: C_2H_2 = 10:1, a reaction temperature of 250 °C, and a reaction pressure of 101 kPa. We evaluated the impact of internal mass transfer using five different particle sizes (80-140, 60-80, 40-60, 20-40, and 10-20 mesh) for the catalysts T-600, T-200, T-H200, and T-H600. After stabilizing the catalyst for 2 hours, we collected three sets of kinetic data for each particle size and catalyst. The experimental results are presented in **Fig. S1b**. as we can see, the reaction rate for TiO_2 catalysts with varying O_V content increases as the catalyst particle size decreases. Specifically, when the catalyst particle size decreases from 10-20 mesh to 40-60 mesh, the reaction rate significantly increases. However, further reduction in particle size to 80-140 mesh results in minimal change in the reaction rate, indicating that internal mass transfer limitations can be neglected when the particle size is below 40-60 mesh. Therefore, using 40-60 mesh particles is sufficient for intrinsic kinetic testing. Additionally, the experiments to eliminate internal and external diffusion effects indicate that the T-H200 catalyst, with an optimal amount of O_V, exhibits the highest reaction rate within the kinetic regime, consistent with our findings under optimal reaction conditions.

3.2 External Diffusion

When considering heat transfer effects, resistance caused by interphase heat transfer can be excluded according to the Mears criterion[6], in which the presence of the interphase heat transfer can be ruled out if the calculated is smaller than 0.15.

$$C_M = \left| \frac{-\Delta H r_{obs} \rho_b R E}{h T^2 R_g} \right|$$

Where ΔH= heat of reaction, kJ/mol

r_{obs}= observed reaction rate, mol/(kg_{cat}·s)

ρ_b = bulk density of catalyst bed, kg/m^3

$= (1 - \Phi)\rho_c$ (Φ=porosity)

R = catalyst particle radius, m

E= activation energy, kJ/mol

h= heat transfer coefficient between gas and pellet, kJ/(m^2·s·K)

R_g= gas constant, kJ/(mol·K)

T = reaction temperature, K

Before determining the heat transfer coefficient(h) for TiO_2-catalyzed semi-hydrogenation of acetylene, the Nusselt number (Nu) and Prandtl number (Pr) for the

catalyst system are calculated with the available value of Reynolds number (Re) according to the following equations:

$$Nu = \frac{hd_p}{k_{t,mix}}$$

$$Pr = \frac{\mu_{mix} C_{p,mix}}{k_{t,mix}}$$

$$Nu = 2 + 0.6 Re^{\frac{1}{2}} Pr^{\frac{1}{3}}$$

Where $k_{t,mix}$ = thermal conductivity of blended reaction gases, kJ/m·s·K,

$C_{p,mix}$ = specific heat of blended reaction gases kJ·kg^{-1}·K^{-1}

μ_{mix} = dynamic viscosity of binary reaction gases, kg·m^{-1}·s^{-1}

dp = average diameter of the catalyst particle, m

For example, using T-H200, the parameters are determined as follows.
ΔH= -175.7 kJ/mol
r_{obs} = 1.4×10^{-4} mol/(kg$_{cat}$·s)
ρ_b = 874.73 kg/m^3
R = 1.5×10^{-4} m
h = 0.65 kJ/(m^2·s·K)
T = 523.15 K
Rg= 8.314×10^{-3} kJ/(mol·K)
E= 11.39 kJ/mol

$k_{t,mix}$ = 2.7932×10^{-5} kJ/(m • s • K)

$C_{p,mix}$= 1.4220 kJ/(kg • K)

dp = 3×10^{-4} m

These parameters are then substituted into the Mears equation.

$$C_M = \left| \frac{-\Delta H r_{obs} \rho_b R E}{h T^2 R_g} \right|$$

= [(176,7 kJ/mol) × (1.4×10^{-4} mol/(kg$_{cat}$·s)×(874.73 kg/m^3)×(1.5×10^{-4} m) × 11.39 kJ/mol]/[(0.65 kJ/(m^2·s·K)) × (523.15 K)^2×8.314×10^{-3} kJ/(mol·K)]
= 2.4855×10^{-5} < 0.15

Since the determined value is much less than the critical value of 0.15, the resistance due to interphase heat transfer can be neglected under our reaction conditions.

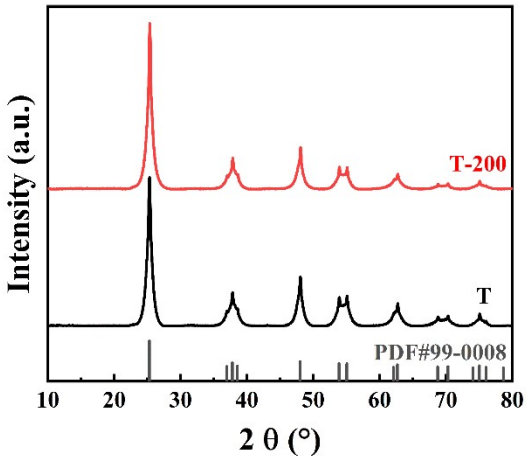

Fig. S2. XRD patterns of untreated commercial titanium dioxide (T) and T-200

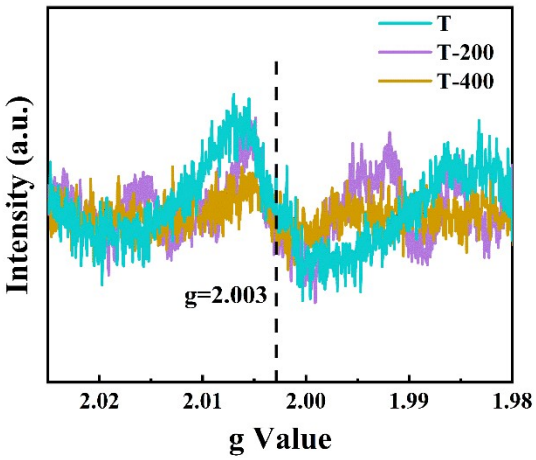

Fig. S3. EPR spectra of T, T-200, and T-400.

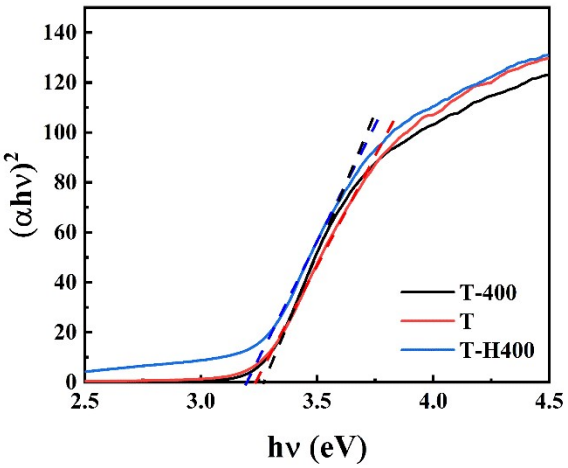

Fig. S4. The $(\alpha hv)^2$ vs hv plots of T-400, T and T-H400, indicating the bandgap for the corresponding absorption spectrum of each sample. Bandgap energy is calculated from the extrapolated line (dashed) fitted to respective linear portions

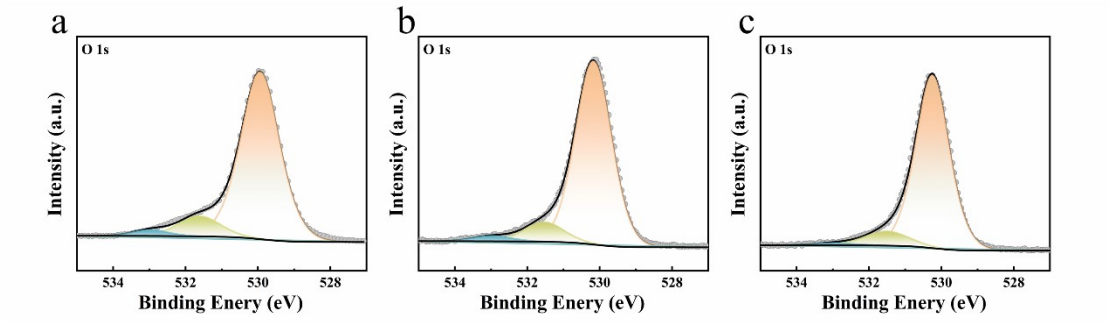

Fig. S5. The O 1s XPS spectra of (a) T-200, (b) T-400, (c) T-600.

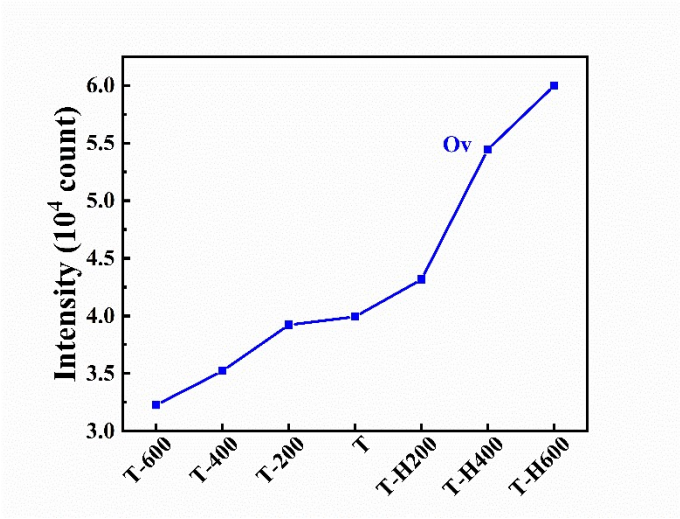

Fig. S6. Variation of the integrated intensity of the O_V peak with TiO_2 catalysts treated under different atmospheres and temperatures.

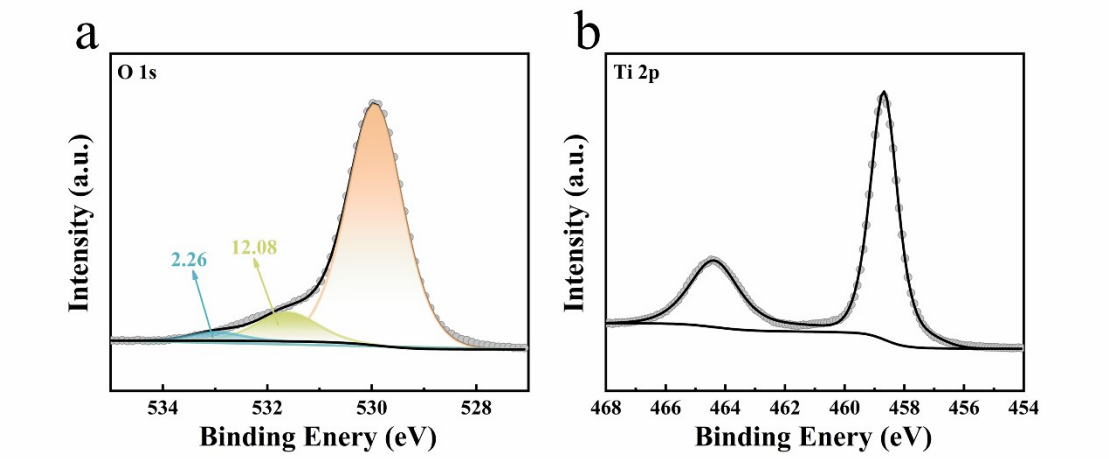

Fig. S7. The O 1s and Ti 2p XPS spectra of Pure TiO_2 without any treatment

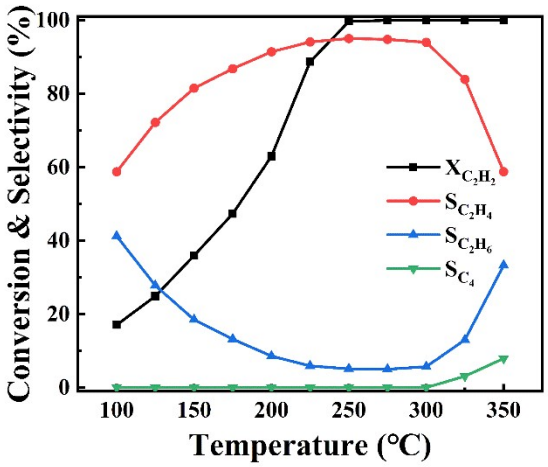

Fig. S8. Evaluation results of T-H200 at different temperatures (Reaction conditions: atmospheric pressure, H_2:C_2H_2=10:1, GHSV=500h^{-1})

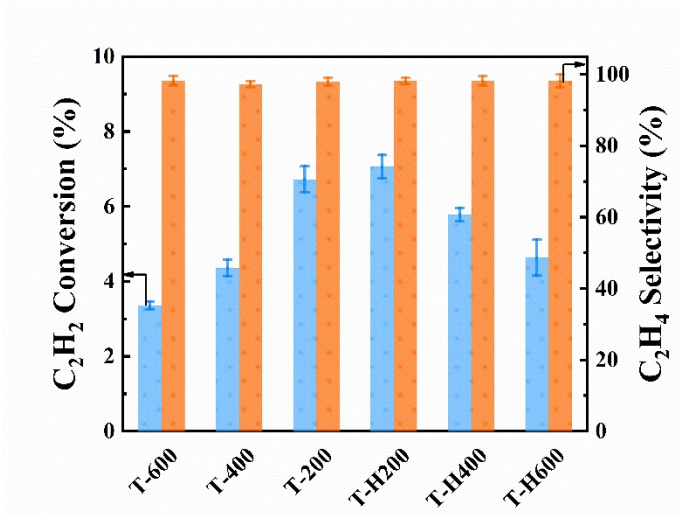

Fig. S9. At low conversion rates (<15%), the conversion and selectivity of different O_V content catalysts in the acetylene hydrogenation reaction were evaluated. (reaction conditions: T = 250°C, F=140 mL·min^{-1} Sv = 54000 h^{-1}, H_2: C_2H_2 = 10: 1, P = 101 kPa).

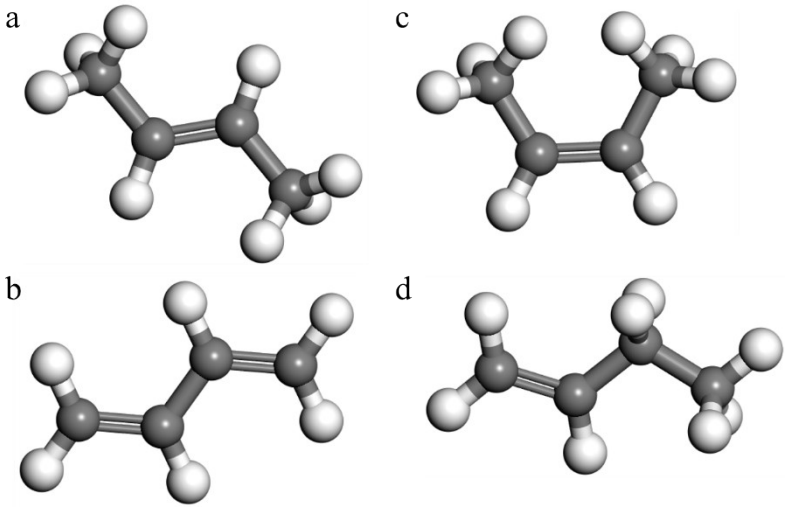

Fig. S10. The main components of C_4 are trans-2-Butene(a), cis-2-Butene(b), 1,3-Butadiene(c) and 1-Butylene(d).

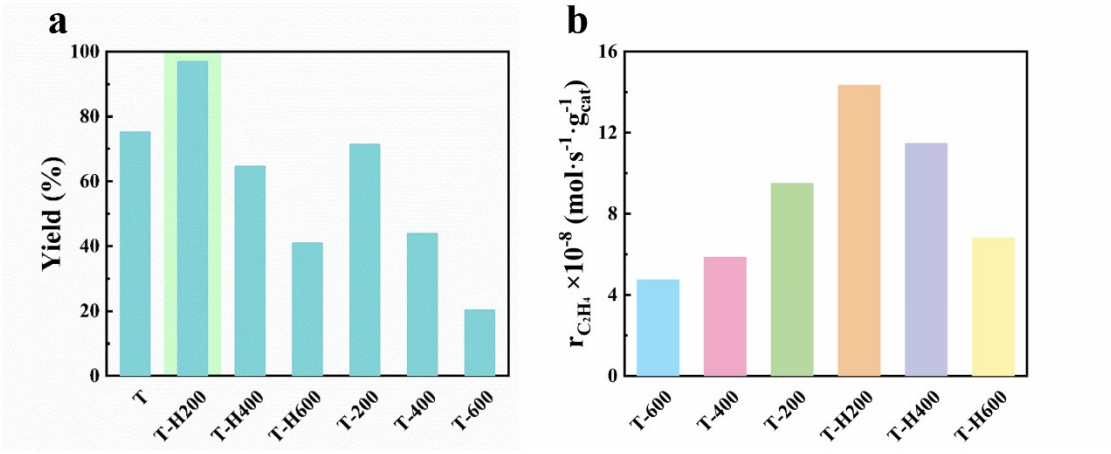

Fig. S11: (a) Yield of TiO2 samples with different OV contents. T, T-H200, T-H400, T-H600, T-200, T-400, and T-600 were 75.08 %, 96.78 %, 64.47 %, 40.84 %, 71.13 %, 43.78 %, and 20.16 %, respectively, and T-H200, which has the highest O_V content, has the highest yield. (b) Ethylene production rate of TiO_2 catalysts with varying O_V content, determined at low conversion (<15%) to ensure the test is within the kinetic range. The O_V contents of the TiO_2 catalysts follow the order T-600 < T-400 < T-H600 < T-200 < T-H400 < T-H200, corresponding to ethylene production rates of 4.71×10^{-8}, 5.82×10^{-8}, 6.76×10^{-8}, 9.46×10^{-8}, 11.44×10^{-8}, and 14.29×10^{-8} mol·s^{-1}·g$_{cat}^{-1}$, respectively. Similar with the acetylene reaction rate, the ethylene production rate is directly proportional to the O_V content, reaching a maximum of 14.29×10^{-8} mol·s^{-1}·g$_{cat}^{-1}$ for the T-H200 sample.

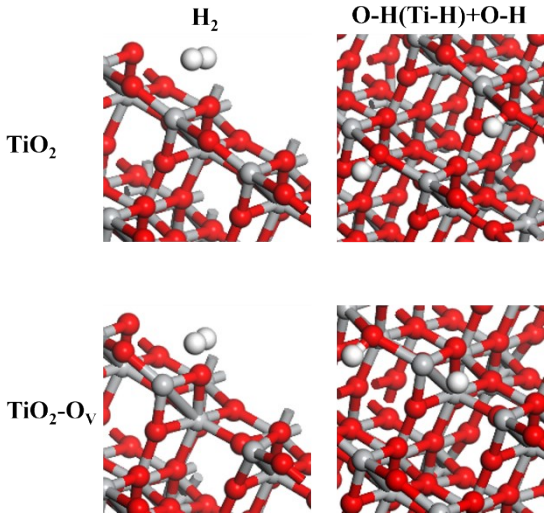

Fig. S12: The initial and transition states of hydrogen on TiO_2 surfaces without O_V (homolytic cleavage) and with O_V (heterolytic cleavage). The red, white, grey and dark grey balls represent O, H, Ti and C atoms, respectively.

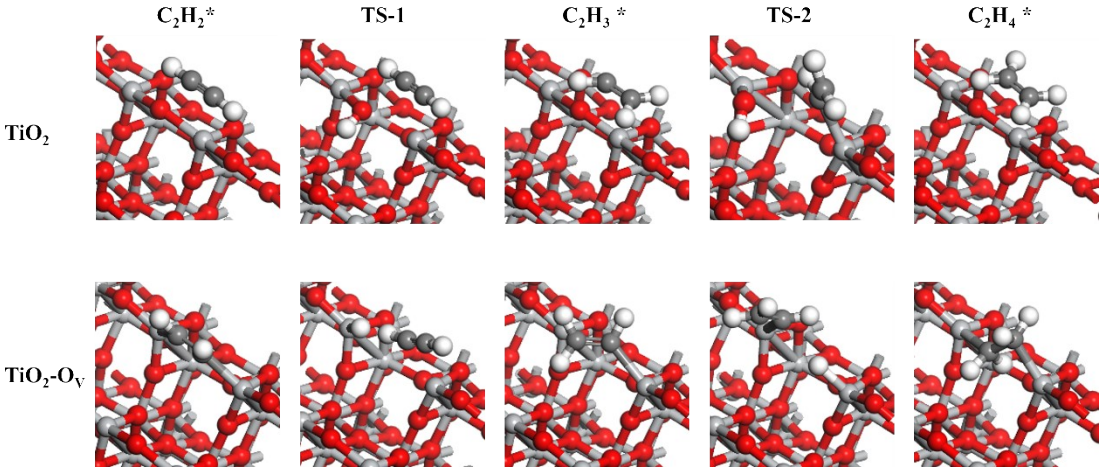

Fig. S13: The semi-hydrogenation process of acetylene between the TiO_2 surface without O_V and the TiO_2 surface with O_V. The red, white, grey and dark grey balls represent O, H, Ti and C atoms, respectively.

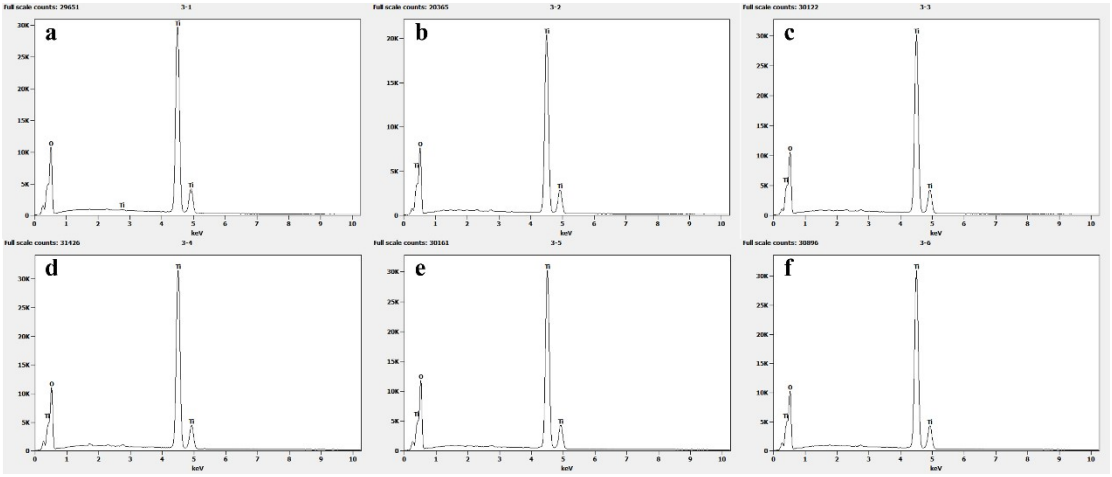

Fig. S14: Elemental analysis of different TiO2 samples (a) T-200, (b) T-400, (c) T-600, (d) T-H200, (e) T-H400 and (f) T-H600.

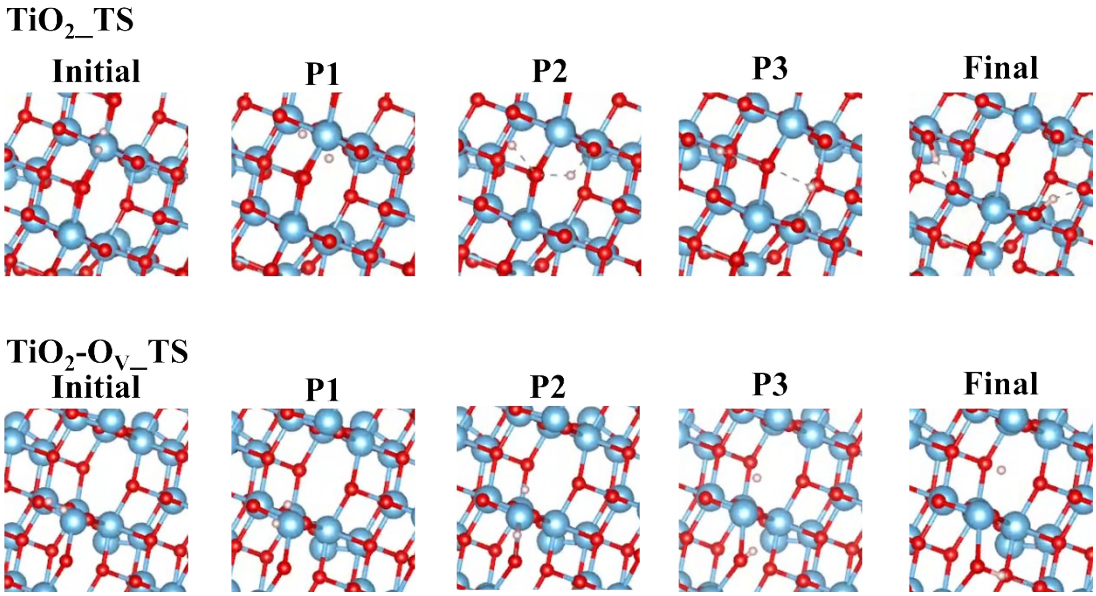

Fig. S15: The initial, transition and final states of H_2 dissociation on TiO_2 and TiO_2-O_V surfaces.

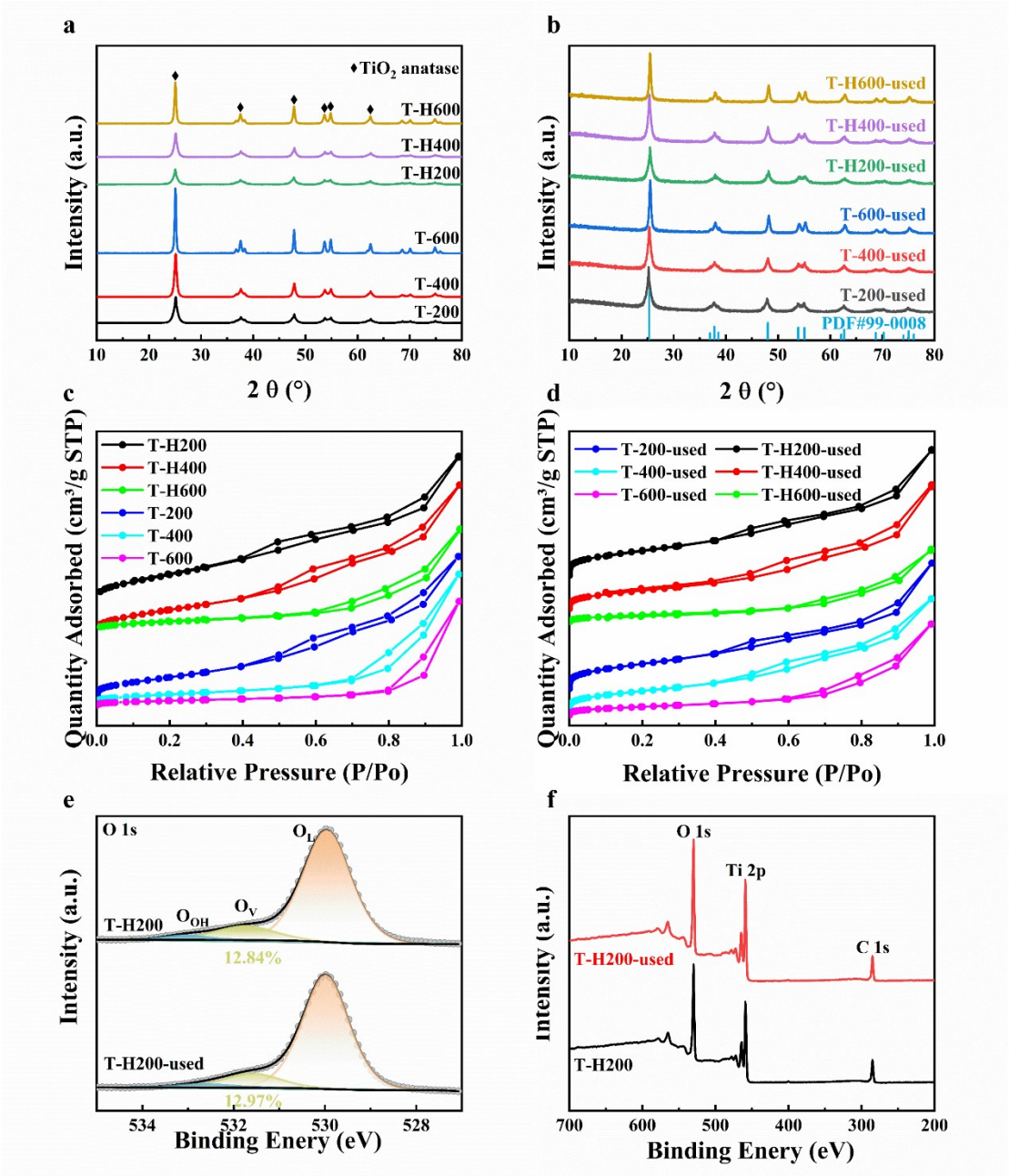

Figure S16: (a) XRD patterns of samples with varying OV content before the reaction and (b) after the reaction. (c) N2 adsorption/desorption isotherms of samples with varying OV content before the reaction and (d) after the reaction. (e) The O 1s XPS spectra of T-H200 before and after the reaction, and (f) the full spectra of T-H200 before and after the reaction.

Table S1. Average crystallite size, BET surface area, proe volume and Proe diameter of TiO_2 Samples

Catalysts	Avg. crystallite size[a] (nm)	BET surface area (m^2/g)	Proe volume (cm^3/g)	Proe diameter (nm)
T-200	10.4	163.23	0.34	8.33
T-400	15.2	70.55	0.30	17.02
T-600	30.6	37.83	0.24	25.32
T-H200	10.9	214.42	0.35	6.58
T-H400	12.3	154.60	0.34	8.84
T-H600	24.5	56.46	0.23	16.25

a. Calculated using the Scherrer equation

Table S2. The relative content of surface lattice oxygen (O_L), oxygen anions near the oxygen vacancy sites (Ov) and hydroxyl species of surface-adsorbed water molecules (O_{OH}).

Sample	O 1s		
	O_L(%)	Ov(%)	O_{OH}(%)
T	85.66	12.08	2.26
T-200	85.93	11.91	2.16
T-400	87.05	10.29	2.66
T-600	88.21	9.10	2.68
T-H200	84.22	12.84	2.94
T-H400	82.49	15.05	2.47
T-H600	79.99	16.70	3.22

Table S3. Reaction energies (Δ E) and energy barriers (Ea) of H_2 dissociation and C_2H_2 hydrogenation.

	H_2* → O-H (Ti-H) + O-H		C_2H_2* + OH (Ti-H) → C_2H_3*		C_2H_3* + O-H → C_2H_4*	
	ΔE	Ea	ΔE	Ea	ΔE	Ea
TiO_2	0.45	1.46	1.89	2.90	4.9	5.03
TiO_2-O_V	-0.55	0.75	-2.98	0.14	-3.13	-1.88

Table S4: Summarized results of publications in acetylene hydrogenation

Catalyst	Composition[a] (vol%) H_2: C_2H_2	Pressure (MPa)	Temperature (^oC)	GHSV (h^{-1})	Durability (h)	Conversion (%)	Selectivity (%)	reaction rates (mol/g/h)	Ref.
ceria−V_O	30: 1	0.1	200	-	-	3.0	12	-	7
ceria−H	30: 1	0.1	200	-	-	2.4	20	-	
ceria−O	30: 1	0.1	200	-	-	7.1	76	-	
TiO_2-H600	-	-	200	-	-	-	-	2×10^{-4}	8
TiO_2-fresh	-	-	200	-	-	-	-	1.1×10^{-4}	
CeO2-673K-O	-	-	150			2.0	96.7	-	
CeO2-533K-H	-	-	150	-	-	1.7	94.7	-	9
CeO2-623K-H	-	-	150	-	-	1.7	94.4	-	
CeO2-673K-H	-	-	150	-	-	2.7	92.4	-	
Pd/TiO2-com-A	1.2: 1	-	40	5400	-	59	58	-	10
T-H200	10: 1	0.1	250	500	23	100	95	6.1×10^{-4}	This work

[a]: The composition refers to the hydrogen-to-acetylene ratio in the presence of excess ethylene.

Table S5: Characteristic Value and Uncertainty of High-Purity Air

Component Name	Standard Value (mol / mol)	Relative Expanded Uncertainty (k = 2)
High-Purity Air	99.999 %	1 %
O_2	20 %∽22 %	
N_2	78 %∽80 %	
H_2	≤ 0.5 ppm	
CH_4	≤ 0.5 ppm	
CO	≤ 0.5 ppm	
CO_2	≤ 0.5 ppm	
H_2O	≤ 3 ppm	

Table S6: Elemental quantitative results of different TiO_2 samples

Sample	Element	Weight (%)	Atom (%)
T-200	O	33.08	59.68
	Ti	66.92	40.32
T-400	O	33.84	60.49
	Ti	66.16	39.51
T-600	O	33.75	60.40
	Ti	66.25	39.60
T-H200	O	32.37	58.89
	Ti	67.63	41.11
T-H400	O	34.60	61.30
	Ti	65.40	38.70
T-H600	O	31.72	58.18
	Ti	68.28	41.82

Table S7: The average grain size, BET surface area, proe volume, and proe diameter of the evaluated TiO_2 samples

Catalysts	Avg. crystallite size[a] (nm)	BET surface area (m^2/g)	Proe volume (cm^3/g)	Proe diameter (nm)
T-200-used	11.1	148.34	0.32	6.64
T-400-used	16.4	64.80	0.29	7.59
T-600-used	31.1	40.36	0.24	12.35
T-H200-used	11.1	166.96	0.32	6.71
T-H400-used	15.1	125.74	0.31	8.52
T-H600-used	26.4	54.51	0.19	11.82

a. Calculated using the Scherrer equation

reference

1 G. Kresse and J. Furthmüller, *Computational Materials Science*, 1996, **6**, 15-50.

2 G. Kresse and J. Hafner, *Physical Review B*, 1994, **49**, 14251-14269.

3 K. Momma and F. Izumi, *J. Appl. Crystallogr.*, 2011, **44**, 1272-1276.

4 Z. Bao, Y. Lu and F. Yu, *AlChE J.*, 2017, **63**, 2019-2029.

5 V. A. Tsipouriari and X. E. Verykios, *Catal. Today*, 2001, **64**, 83-90.

6 D. E. Mears, *Industrial & Engineering Chemistry Process Design and Development*, 1971, **10**, 541-547.

7 Z. Li, L. Chen, Z. Wu, A. Jia, S. Shi, H. Zhang, J. Wang, Z. Liu, W.-P. Shao, F. Yang, X.-P. Wu, X.-Q. Gong and W. Huang, *ACS Catalysis*, 2023, **13**, 5213-5224.

8 Q. Wan, Y. Chen, S. Zhou, J. Lin and S. Lin, *J. Mater. Chem. A*, 2021, **9**, 14064-14073.

9 J. Moon, Y. Cheng, L. L. Daemen, M. Li, F. Polo-Garzon, A. J. Ramirez-Cuesta and Z. Wu, *ACS Catalysis*, 2020, **10**, 5278-5287.

10 J. Panpranot, K. Kontapakdee and P. Praserthdam, *Applied Catalysis A: General*, 2006, **314**, 128-133.